Human Molecular Genetics, 2014, Vol. 23, No. 11 **2981–2994**
doi:10.1093/hmg/ddu009
Advance Access published on January 12, 2014

Zebrafish Cacna1fa is required for cone photoreceptor function and synaptic ribbon formation

Sujuan Jia[1], Akira Muto[2,†], Wilda Orisme[1], Hannah E. Henson[1,3], Chaithanyarani Parupalli[1], Bensheng Ju[1], Herwig Baier[2,‡] and Michael R. Taylor[1,*]

[1]Department of Chemical Biology and Therapeutics, St Jude Children's Research Hospital, Memphis, TN 38105, USA, [2]Department of Physiology, University of California, San Francisco, CA 94158, USA and [3]Integrated Program in Biomedical Sciences, University of Tennessee Health Science Center, Memphis, TN 38163, USA

Received October 9, 2013; Revised December 23, 2013; Accepted January 8, 2014

Mutations in the human *CACNA1F* gene cause incomplete congenital stationary night blindness type 2 (CSNB2), a non-progressive, clinically heterogeneous retinal disorder. However, the molecular mechanisms underlying CSNB2 have not been fully explored. Here, we describe the positional cloning of a blind zebrafish mutant, *wait until dark* (*wud*), which encodes a zebrafish homolog of human CACNA1F. We identified two zebrafish *cacna1f* paralogs and showed that the *cacna1fa* transcript (the gene mutated in *wud*) is expressed exclusively in the photoreceptor layer. We demonstrated that Cacna1fa localizes at the photoreceptor synapse and is absent from *wud* mutants. Electroretinograms revealed abnormal cone photoreceptor responses from *wud* mutants, indicating a defect in synaptic transmission. Although there are no obvious morphological differences, we found that *wud* mutants lacked synaptic ribbons and that *wud* is essential for the development of synaptic ribbons. We found that Ribeye, the most prominent synaptic ribbon protein, was less abundant and mislocalized in adult *wud* mutants. In addition to cloning *wud*, we identified *synaptojanin 1* (*synj1*) as the defective gene in *slacker* (*slak*), a blind mutant with floating synaptic ribbons. We determined that Cacna1fa was expressed in *slak* photoreceptors and that Synj1 was initially expressed *wud* photoreceptors, but was absent by 5 days post-fertilization. Collectively, our data demonstrate that Cacna1fa is essential for cone photoreceptor function and synaptic ribbon formation and reveal a previously unknown yet critical role of L-type voltage-dependent calcium channels in the expression and/or distribution of synaptic ribbon proteins, providing a new model to study the clinical variability in human CSNB2 patients.

INTRODUCTION

Photoreceptor cells have the amazing ability to respond and adapt to a wide range of light intensities (1). To transmit this dynamic visual information, their presynaptic terminals form specialized structures called synaptic ribbons, which are present in retinal rod and cone photoreceptor cells, bipolar cells and inner ear sensory hair cells (2). Although multiple roles have been proposed, it is widely believed that ribbons function as molecular conveyor belts for synaptic vesicles and the tonic release of the neurotransmitter glutamate (3–6). Great progress has been made over recent years in identifying many of the key components required for synaptic ribbon structure (3,7,8). For example, targeted deletion of murine homolog for synaptic ribbon protein BASSOON results in unanchored 'floating' ribbons and impaired synaptic transmission (9). Mutations in zebrafish *synaptojanin1* also cause floating ribbons due to its role in ribbon anchoring (10–13). In addition, morpholino knockdown of zebrafish *ribeye a* results in shorter and fewer synaptic ribbons (14). While our understanding synaptic ribbons has expanded, much remains unknown regarding the complex interactions among these proteins and how they affect ribbon synaptogenesis.

*To whom correspondence should be addressed at: Department of Chemical Biology and Therapeutics, St. Jude Children's Research Hospital, 262 Danny Thomas Place, MS1000, Memphis, TN 38105, USA. Tel: +1 9015956269; Fax: +1 9015955715; Email: michael.taylor@stjude.org
†Present address: Division of Molecular and Developmental Biology, National Institute of Genetics, 1111 Yata, Mishima, Shizuoka 411-8540, Japan.
‡Present address: Genes – Circuits – Behavior, Max Planck Institute of Neurobiology, Am Klopferspitz 18, 82152 München-Martinsried, Germany.

Photoreceptor L-type voltage-dependent calcium channels (L-VDCCs) are found adjacent to synaptic ribbons and are required for calcium influx and synaptic vesicle fusion (4,15). The essential role of these channels for visual function is clearly evident in the human retinal disease X-linked congenital stationary night blindness type 2 (CSNB2), where dozens of mutations have been identified in the *CACNA1F* gene (16–18). Electroretinograms (ERGs) from these patients indicate that synaptic transmission from rod photoreceptors is diminished and cone photoreceptors function is abnormal (19). The *nob2* (*no b-wave 2*) mouse model also results in abnormal synaptic transmission and a profound loss of rod photoreceptor synapses (20), although recent studies have shown that *nob2* is not a complete knockout of *Cacna1f* (21).

In contrast to *nob2*, complete knockout of mouse *Cacna1f* results in cone photoreceptor degeneration, a phenotype not found in human CSNB2 patients. Thus, due to the loss of cones in the complete mouse knockout, little is known about the function of L-VDCCs in ribbon synapses of cone photoreceptors.

Here, we report that the blind zebrafish mutant *wait until dark* (*wud*) encodes a homologue of human *CACNA1F* and that the *slak* mutant encodes Synaptojanin 1 (Synj1). Our results indicate that zebrafish *cacna1fa* is essential for proper synaptic ribbon formation and cone photoreceptor function due to an important role in regulating the expression and localization of synaptic ribbon proteins. We propose that our zebrafish model provides a novel tool for studying L-VDCCs in cone photoreceptors that may advance our understanding of the clinical variability in human CSNB2 patients.

RESULTS

wud has a thinner outer plexiform layer and defective ERGs

wud was identified in a large-scale mutagenesis screen for defects in visual behavior, where five *wud* alleles were isolated (22). *wud* mutants showed normal external morphology, visual background adaptation and spontaneous swimming activity, but completely lacked an optokinetic response (OKR) and optomotor response (OMR), indicating that *wud* mutants were blind. As a recessive mutation, *wud* follows Mendelian inheritance; where one-quarter of the offspring from heterozygous parents are OKR and OMR negative. Despite the loss of sight, *wud* mutants are adult viable, indicating that the *wud* gene is not essential for survival but for visual function. Behaviorally, adult *wud* mutants are blind in bright and dim light, indicating that both cone and rod function are defective (data not shown). They show no startle response and generally remain near the bottom of their tank where they forage for settled food and do not eat following visual cues, a behavior that is clearly evident in wild-type adults. Because the visual system of zebrafish larvae younger than 15 days postfertilization (dpf) rely entirely on cones and not rods (23), the *wud* mutation appeared to affect cone photoreceptor function and/or the processing of cone photoreceptor signals.

To examine retinal morphology, we performed immunohistochemistry (IHC) with zpr1 and PKC antibodies, which label cone photoreceptor cells and bipolar cells, respectively. This analysis did not reveal any significant differences between wild type and *wud* (Fig. 1A–F). However, we noted that the outer plexiform layer (OPL) appeared thinner in *wud* when compared with wild-type siblings. The OPL is the first synaptic layer in retina where photoreceptors connect with dendrites of bipolar and horizontal cells, forming a unique neurosensory structure called a ribbon synapse (1,4). To examine the OPL more closely, we measured the thickness of the OPL in wild-type and mutant larvae. As shown in Figure 1G–J, the OPL was significantly thinner in *wud* ($2.12\ \mu m \pm 0.18$, $n = 26$) compared with wild type ($3.54\ \mu m \pm 0.12$, $n = 24$) (Fig. 1K). This led us to conclude that the *wud* gene may encode a protein that localizes to cone photoreceptor synapses.

To examine the physiology of the *wud* outer retina, we performed ERGs. ERGs are commonly used as an indicator of outer retina function and are comprised a small negative-going a-wave arising from the photoreceptors and a large-positive-going b-wave arising from depolarizing ON bipolar cells. For these experiments, we recorded from dark-adapted wild-type and *wud* larvae at 5–6 dpf in response to a 20 ms flash of white light. As shown in Figure 2, wild-type larvae show stereotypical responses that increase in amplitude with brighter light intensities. In contrast, *wud* showed that abnormal ERGs comprise a small a-wave followed by a delayed and reduced b-wave consistent with a defect in synaptic transmission from cone photoreceptors. Unexpectedly, we also found an additional slow, positive-going component of the *wud* ERG that increased with light intensity. Application of the glutamate analog APB, which blocks photoreceptor synaptic transmission (24), did not affect this positive component (data not shown), indicating that this response is likely arising from the defective cone photoreceptors and not bipolar cells. To demonstrate that this was not an electrical artifact, we recorded from the zebrafish *pde6c*^{w59} mutant that has a mutation in the cone-specific *phosphodiesterase 6c* gene (25). As expected, these recordings showed flat traces consistent with phototransduction defects and photoreceptor degeneration in the *pde6c*^{w59} mutant. Thus, our results indicate that *wud* has a defective ERG indicative of a synaptic transmission defect as well as additional abnormalities.

wud encodes Cacna1fa

To identify the defective gene in *wud*, we used a positional cloning strategy. *wud* was initially mapped to linkage group (LG) 8 using microsatellite markers (22). Fine mapping by recombination analysis defined a critical interval of 4.7 Mb between markers z789 and z15786, encompassing ~75 known and 13 novel genes by examining the zebrafish genome at the ensembl.org website (Fig. 3A). Database mining within this region identified a zebrafish gene with strong homology to human *CACNA1F*. Because mutations in *CACNA1F* cause human retinal disease, we considered this zebrafish ortholog as a strong candidate for the *wud* gene. Consistent with a whole-genome duplication event in zebrafish, we identified two paralogs of human *CACNA1F* that we named *cacna1fa* (the *wud* gene) and *cacna1fb* (~23 Mb proximal to the *wud* locus). Sequence alignment of the predicted proteins showed that zebrafish Cacna1fa (also called $Ca_v1.4a$, encoded by *cacna1fa*) and Cacna1fb (encoded by *cacna1fb*) are 62.8% and 55.5% identical to human $Ca_v1.4$, respectively. The open reading frame of the *cacna1fa* transcript contains 6345 bp that encode a 2115

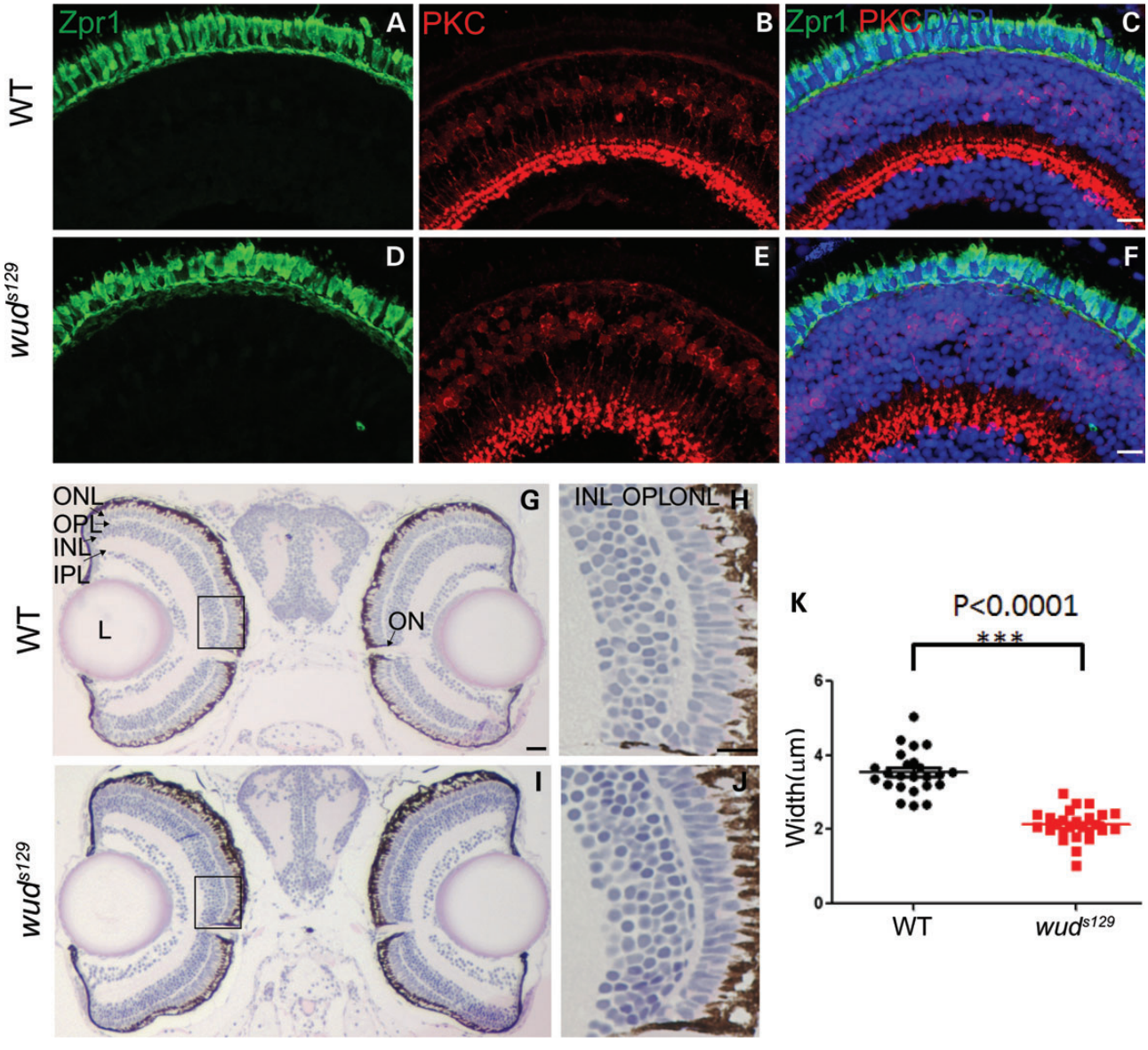

Figure 1. *wud* mutants have a thinner outer plexiform layer. (**A**–**F**) IHC revealed relatively normal retinal morphology. Larvae at 7 dpf were stained with zpr1 (A and D), which labels double cones, and PKC (B and E), which labels bipolar cells. Nuclei were counterstained with DAPI in the merged images (C and F). (**G**–**K**) *wud* mutants have a thinner outer plexiform (OPL) layer. Shown here are H&E stained semi-thin plastic sections of wild-type (G) and *wud* (I) larvae at 7 dpf. Magnified views of the boxed areas in G and I are shown in H and J, respectively. Measurements ($n = 24$ per group) revealed a significantly thinner OPL (K, $P < 0.0001$). ONL, outer nuclear layer; OPL, outer plexiform layer; INL, inner nuclear layer; IPL, inner plexiform layer; L, lens; ON, optic nerve. Scale bars for C, F and H is 10 μm and G is 20 μm.

amino acid protein with a predicted molecular weight of 232 kDa and protein domains highly similar to those of other vertebrate $Ca_v1.4$ proteins (Fig. 3B). By sequencing *cacna1fa* cDNA, we discovered a 626T > A transversion mutation in the *wud*^{s129} allele and a 3403C > T transition mutation in the *wud*^{s315} allele that resulted in premature stop codons L209X and Q1135X, respectively (Fig. 3B). No mutations were found in *cacna1fb* or any other candidate genes examined.

To examine the expression pattern of the zebrafish *cacna1f* genes, we performed whole-mount *in situ* hybridization (WISH) on wild-type larvae. Because the zebrafish retina becomes functional at 3 dpf, we examined the expression of *cacna1f* transcripts at this stage. As shown in Figure 3, both *cacna1fa* and *cacna1fb* were expressed at high levels within the retina with little or no expression outside of the eye. These transcripts were expressed in mutually exclusive patterns. *cacna1fa* expression was restricted to the outer retina in a pattern consistent with photoreceptor expression (Fig. 3C and D), whereas *cacna1fb* expression was localized to the inner retina (Fig. 3E and F). Given the cone-dominated retina of larval zebrafish and the divergent expression pattern of the duplicated *cacna1f* genes, the *wud* mutant provides a unique tool for *cacna1fa* loss-of-function studies specifically in cone photoreceptors.

To examine Cacna1f protein expression, we generated a polyclonal antibody against a C-terminal fragment of Cacna1fa

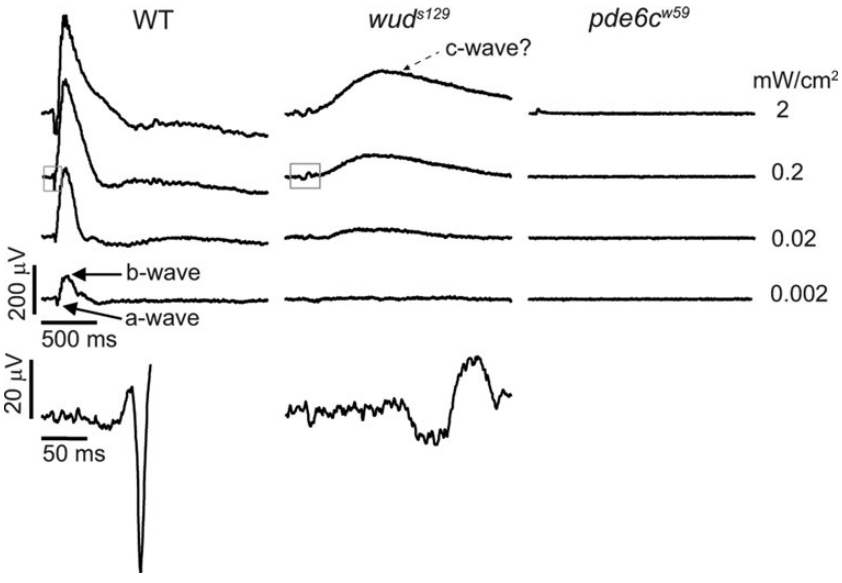

Figure 2. *wud* mutants display abnormal ERGs. Wild-type larvae showed stereotypical ERGs across 4 log units of illumination (flash intensities are shown on the right). The a- and b-wave components of the ERG are indicated in the dimmest trace (bottom left). *wud* mutants showed defective ERGs with significantly reduced sensitivity. These waveforms comprise a small a-wave followed by a delayed and reduced b-wave and a slow, large-positive component that may represent a c-wave indicated on the top *wud* trace. No ERG responses were recorded from the *pde6c* mutants, although a miniscule flash artifact can be seen on the brightest trace (top, right trace). Close-ups of the boxed regions from the second wild-type and *wud* traces are shown on the bottom to illustrate the magnitude of the a-wave and the delay of the b-wave.

(Fig. 3B). Using IHC, we detected Cacna1fa specifically in the OPL of wild-type larvae at 7 dpf. This staining pattern was consistent with our WISH results (Fig. 3C and D) and confirmed that Cacna1fa was expressed only in the OPL and not across multiple layers of the retina as in mammals (18). As expected, we did not detect Cacna1fa in either *wud* allele, which is in agreement with both mutants as null alleles that do not express functional Cacna1fa protein (Fig. 4A). However, since our antibody was designed near the C-terminus, we cannot rule out the possibility that a truncated protein is expressed in the mutants. Because no differences were observed between the two *wud* alleles in visual behavior, protein expression, morphology or physiology, the subsequent experiments were performed with wud^{s129}. We next examined Cacna1fa in adult zebrafish using IHC. As with the larval IHC, we detected a strong signal in the OPL of wild-type adults, but no signal in the OPL of *wud* mutants (Fig. 4B). To demonstrate the specificity of our Cacna1fa antibody, we performed western blots on wild-type and *wud* adult eye extracts. We observed a single band at ∼232 kDa in the wild-type extract and no detectable band in the *wud* mutant extract (Fig. 4C). The specificity of this antibody was further confirmed by antigen competition experiments (data not shown).

Cacna1fa is required for the development of cone synaptic ribbons

Although mutations in the mouse *Cacna1f* gene are known to result in abnormal rod photoreceptor synapses (26,27), little is known about structural defects in cones. Therefore, we analyzed the ultrastructure of cone photoreceptor synapses in *wud* mutants by transmission electron microscopy (TEM). In wild-type adults, we observed normal cone pedicles with invaginating dendrites from presumptive bipolar and horizontal cells along with stereotypical synaptic ribbons attached to the presynaptic membrane and projecting perpendicular into the cone terminal (Fig. 5A and B). In contrast, cone pedicles in *wud* adults displayed little or no dendritic invagination and a complete absence of synaptic ribbons (Fig. 5C and D). These results are consistent with previous studies demonstrating loss of rod synaptic ribbons in *Cacna1f* knockout mice (26,27). However, we noticed small particles in the *wud* cone pedicle, absent in wild type, which resembled small round precursor bodies (srPBs) (10).

Because no synaptic ribbons were detected in *wud* cone photoreceptors by TEM, we examined the expression of Ribeye, the main component of synaptic ribbons and the only known protein unique to this structure (28). In addition to its structural role, it has been suggested that Ribeye is essential for the formation of synaptic ribbons (29,30). Similar to *cacna1f*, zebrafish have two *ribeye* genes that are both expressed in the retina with *ribeye b* expressed specifically in photoreceptors (14). Using an antibody specific to Ribeye b (31), we found that Ribeye b was specifically expressed in the OPL of wild-type adults and colocalized with the synaptic vesicle protein SV2 (Fig. 6A–D). In contrast, Ribeye b expression was significantly reduced in the OPL of *wud*, showed little colocalization with SV2 and appeared to be mislocalized to the photoreceptor inner segments (Fig. 6E–H). We found no significant difference in *ribeye b* mRNA levels between wild type and *wud* as determined by quantitative RT-PCR (Fig. 6I). Our data indicate role for Cacna1fa in the expression and localization of Ribeye b that appears to be independent of transcriptional regulation.

To address whether the adult synaptic phenotype in *wud* is a developmental or a degenerative process, we examined the initial formation of cone synaptic ribbons. We predicted that if Cacna1fa were essential for the initial stages of ribbon

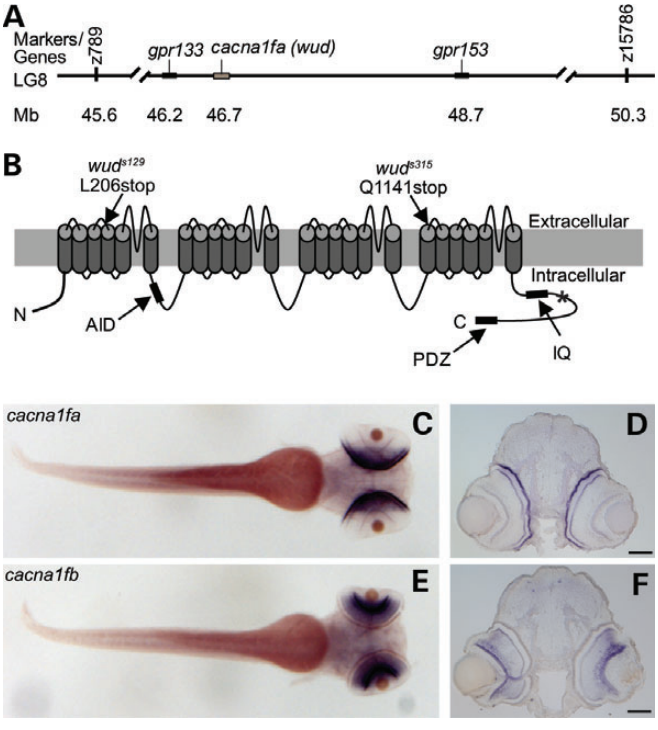

Figure 3. *wud* encodes Cacna1fa and is expressed in cone photoreceptors. (**A**) Genetic map of *wud* locus on zebrafish LG 8 showing the genetic markers and neighboring genes. (**B**) Schematic of the zebrafish Cacna1fa protein showing the location of the *wud* mutations. The channel contains four repeated domains each of which contains each six transmembrane regions, an alpha interacting domain (AID), an IQ domain and a PDZ domain at the C-terminus. The approximate position of the antibody epitope is labeled with an asterisk. Two independent alleles of *wud* (s129 and s315) were sequenced and both were found to have premature stop codons predicted to result in null mutations. (**C**–**F**) WISH of *cacna1fa* (C and D) and *cacna1fb* (E and F) at 3 dpf showed expression in the photoreceptor layer and inner retina, respectively. (C) and (E) show whole mounts and (D) and (F) show retinal cryosections of (C) and (E), respectively. Scale bar: (B), 50 μm.

development, then *wud* mutants would never form ribbons. Alternatively, if Cacna1fa were not essential for ribbon development, then we would expect to observe the initial formation of ribbons followed by degeneration/disassembly, indicating that Cacna1fa plays a role in ribbon maintenance not formation. Previous studies in zebrafish have demonstrated that functional ribbons arise within cone photoreceptor synaptic terminals at 65 h postfertilization (hpf) (10). Therefore, we examined wild-type and mutant larvae just before and after this developmental milestone. As expected, no ribbons were observed in wild type or mutant at 60 hpf (Fig. 7A–D), yet invaginated processes were observed in the wild-type pedicle (Fig. 7B). However, by 72 hpf, synaptic ribbons were clearly present in wild-type larvae ($n = 3$), but were absent in *wud* mutants ($n = 5$) (Fig. 7E–H), indicating that Cacna1fa is necessary for the initial formation of synaptic ribbons. We did not uncover any evidence of delayed ribbon formation at a later developmental time point (Fig. 7I–L), further supporting the essential role of Cacna1fa in synaptic ribbon development.

Calcium influx through calcium channels initiates many different cellular processes (32). In fact, it has been shown that $Ca_v1.3$ regulates the size of synaptic ribbons in sensory hair cells and the pineal gland (33). To further examine the role of calcium influx on the expression of photoreceptor ribbon proteins, we treated wild-type larvae with isradipine, an antagonist of L-type calcium channels and examined Ribeye b expression. Previous studies have demonstrated that synaptic ribbons are very dynamic organelles, where, in fish, synaptic ribbons form in the day and disaggregate at night (10,34). Thus, for this experiment, wild-type larvae were dark-adapted to disaggregate synaptic ribbons, then placed in light for 1 h to allow ribbons to form in the presence or absence of isradipine. As shown in Figure 6, we found that Ribeye b was expressed in the OPL of control larvae (dimethylsulfoxide, DMSO) (Supplementary Material, Fig. S1A and B), but was significantly reduced in the OPL of isradipine-treated larvae (Supplementary Material, Fig. S1C and D). These data indicate that calcium influx is necessary for the proper expression of the most prominent synaptic ribbon protein in cone photoreceptors.

slacker encodes synj1

The *slacker*^{s564} (*slak*) mutant was isolated from the same large-scale visual behavior screen that identified *wud* and was genetically mapped to LG10 (22). Besides having no OKR, *slak* also has a loss-of-balance phenotype indicative of a vestibular defect (35). To further characterize this mutant, we performed TEM and found that *slak* had floating synaptic ribbons at 7 dpf (Fig. 8A and B). Due to the map position and the phenotype, we predicted that *slak* could be a new allele of *synj1*. To test this idea, we performed a complementation test with *nrc*, a mutant with a premature stop codon in *synj1* (11). We found that *slak* failed to complement *nrc*, which indicated that *slak* was a new allele of *synj1*. Sequencing of *synj1* cDNA from *slak* mutants revealed a deletion of 14 nucleotides between exon 20 and exon 21. Subsequent sequencing of genomic DNA from *slak* confirmed a single nucleotide change in the splice donor site of intron 20 (G to A, Fig. 8C), which generated a frame shift due to a cryptic splice donor site and resulted in a premature stop codon in exon 21 that truncates the protein at amino acid 926 (Fig. 8D).

To examine Synj1 protein expression, we performed IHC on *slak* larvae using both a zebrafish Synj1-specific antibody (13) and our Cacna1fa-specific antibody. As previously demonstrated for the *nrc* allele (13), we found strong expression of Synj1 in both the OPL and IPL of wild-type larvae (Fig. 8E and G). We found no detectable Synj1 in the OPL or IPL from *slak* mutants (Fig. 8H and J), indicating that *slak* is likely a null allele of *synj1*. Because synaptic ribbons form in *synj1* mutants, we predicted that the expression and localization of Cacna1fa would be normal in *synj1* mutants. Indeed, we found that Cacna1fa was detectable at similar levels in the OPL of both wild-type larvae (Fig. 8F and G) and *slak* mutants (Fig. 8I and J), indicating that Synj1 is not required for the expression or localization of Cacna1fa. The presence of Cacan1fa in the OPL of *slak* mutants, which have ribbons at the synapse (albeit unattached), supports the essential role of Cacna1fa in photoreceptor synaptic ribbon formation.

Synj1 plays an important role in synaptic ribbon function, especially in photoreceptor synaptic ribbon anchoring (11–13). We predicted that the expression of Synj1 in *wud* mutants might be affected due to the absence of photoreceptor

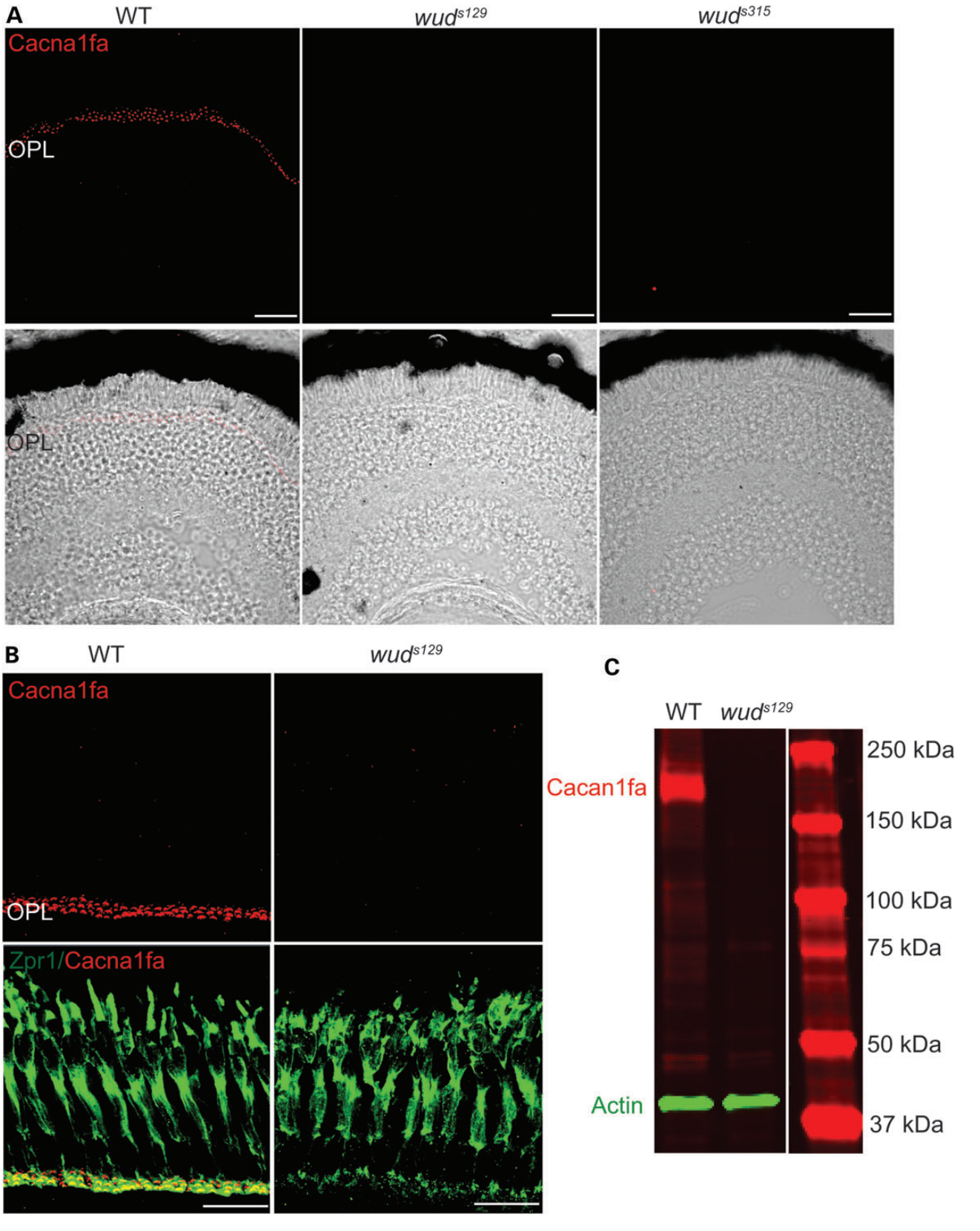

Figure 4. Cacna1fa is expressed in wild-type OPL and is absent from *wud* mutants. (**A**) Cacna1fa was detected specifically in the OPL of wild-type (WT) retina (7 dpf). Cacnaf1a was not detectable in either *wud*^{s129} or *wud*^{s315}. (**B**) Cacna1fa is localized at the synaptic terminal of photoreceptors in adult wild-type retina. (**C**) Immunoblot analysis of Cacna1fa (red) from adult wild-type and *wud*^{s129} mutant eye extracts. Actin (green) was used as an internal reference for gel loading.

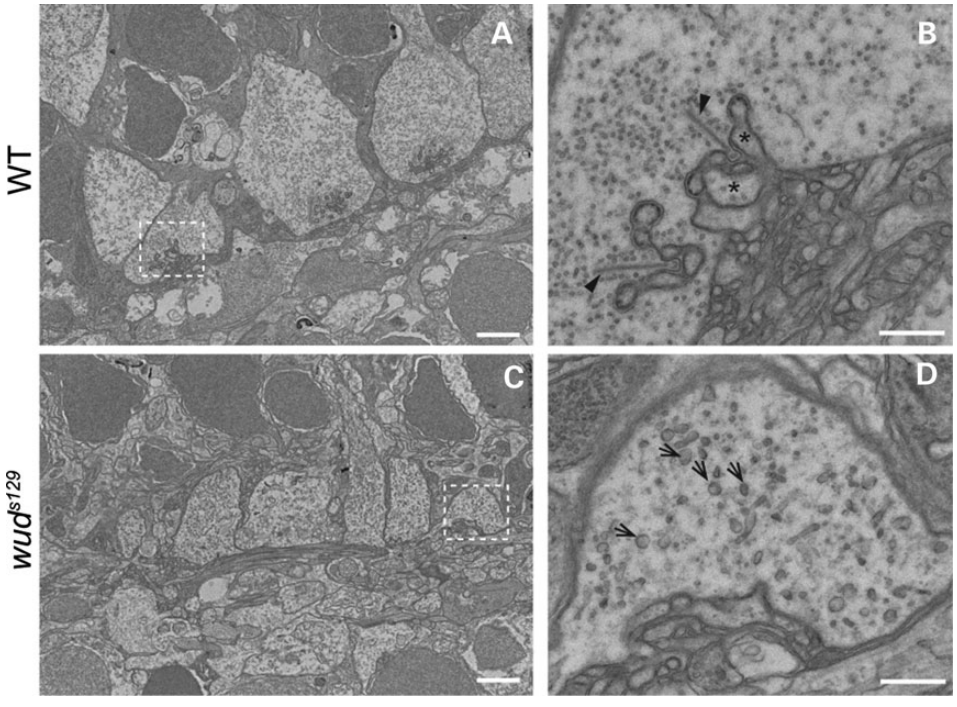

Figure 5. Synaptic ribbons are absent in *wud* mutants. (**A–D**) Transmission electron microscopy of adult wild-type and *wud* mutants. In wild type (WT), the cone pedicles showed dendritic invaginations and multiple docked synaptic ribbons (A and B). In (B) horizontal cells (asterisks) and synaptic ribbons (arrowheads) are indicated. In contrast, the *wud* mutants had abnormal cone pedicles that lacked dendritic invaginations and synaptic ribbons (C and D). srPB were observed in the *wud* mutants (arrows in D). Scale bar: (A) and (C), 2 μm; (B) and (D), 500 nm.

synaptic ribbons. As expected, Synj1 colocalized with Cacna1fa in the OPL of wild-type larvae at 3 and 5 dpf (Supplementary Material, Fig. S2A–C and G–I). Synj1 was initially expressed in both the OPL and IPL of *wud* mutants at 3 dpf (Supplementary Material, Fig. S2D–F), when the photoreceptors and synaptic ribbons begin to form. However, the expression of Synj1 was undetectable in the OPL of *wud* mutants at 5 dpf and at later stages (Supplementary Material, Fig. S2J–L). Furthermore, we examined the expression of Synj1 wild-type larvae treated with isradipine to determine if Synj1 expression is regulated by calcium influx. We found that the expression of Synj1 is significantly decreased in the isradipine-treated larvae (Supplementary Material, Fig. S2O and P). These data suggest that calcium influx via Cacna1fa is not essential for the initial expression of Synj1, but that calcium influx is likely required for the sustained expression of Synj1.

DISCUSSION

In this study, we demonstrate that the molecular defects associated with blindness in the *wud* mutant are due to mutations in an L-VDCC gene, *cacna1fa*. Given that: (i) we uncovered premature stop codons in *cacna1fa* from two independent alleles of the *wud* mutant; (ii) mutations in the human *CACNA1F* gene cause retinal disease; (iii) the expression pattern of wild-type *cacna1fa* is localized to zebrafish photoreceptors and is absent from *wud* mutants; (iv) *wud* mutants display abnormal ERGs and (v) cone synaptic ribbon formation is defective in *wud* mutants, we have conclusively demonstrated that the *wud* mutant phenotype is due to mutations in *cacna1fa*.

We identified two zebrafish paralogs of human *CACNA1F*, *cacna1fa* and *cacna1fb*. Due to a whole-genome duplication event in zebrafish, many zebrafish genes have one or more paralogs that either have overlapping function and expression or have distinct patterns of expression. Interestingly, both zebrafish *cacna1f* genes appear to be expressed in the retina in mutually exclusive patterns and are located in two separate synaptic layers in the retina. In mice, *Cacna1f* is expressed in multiple layers of the retina, including the OPL and IPL (27). This expression pattern is consistent with the distribution of synaptic ribbons in both photoreceptors and bipolar cells (2). However, in zebrafish, it appears that the *cacna1f* gene was duplicated into two-independent genes with distinct expression patterns. This finding could be a great advantage for studying the function of Cacna1fa specifically in cone photoreceptors without the complication of bipolar cell involvement.

CACNA1F ($Ca_v1.4$) is known to play an important role in photoreceptor synaptic transmission. As mentioned previously, mutations in the human *CACNA1F* gene cause CSNB2 and cone-rod dystrophy (16–18,36). CSNB2 represents a clinically variable group of low vision disorders characterized by abnormal ERGs, impaired night vision, reduced visual acuity, myopia, nystagmus and strabismus (37–39). Studies in mice have shown that Cacna1f is vital for the functional assembly and/or maintenance of rod photoreceptor ribbon synapses (27). This study also showed a profound loss of cone photoreceptor function as demonstrated by ERG, although it is unclear how and why cones are affected in this model. Unlike the rod-dominant retina in mice, zebrafish have a cone-dominated retina, comparable with the fovea of the human retina, making zebrafish a complementary model for retinal diseases. Synaptic

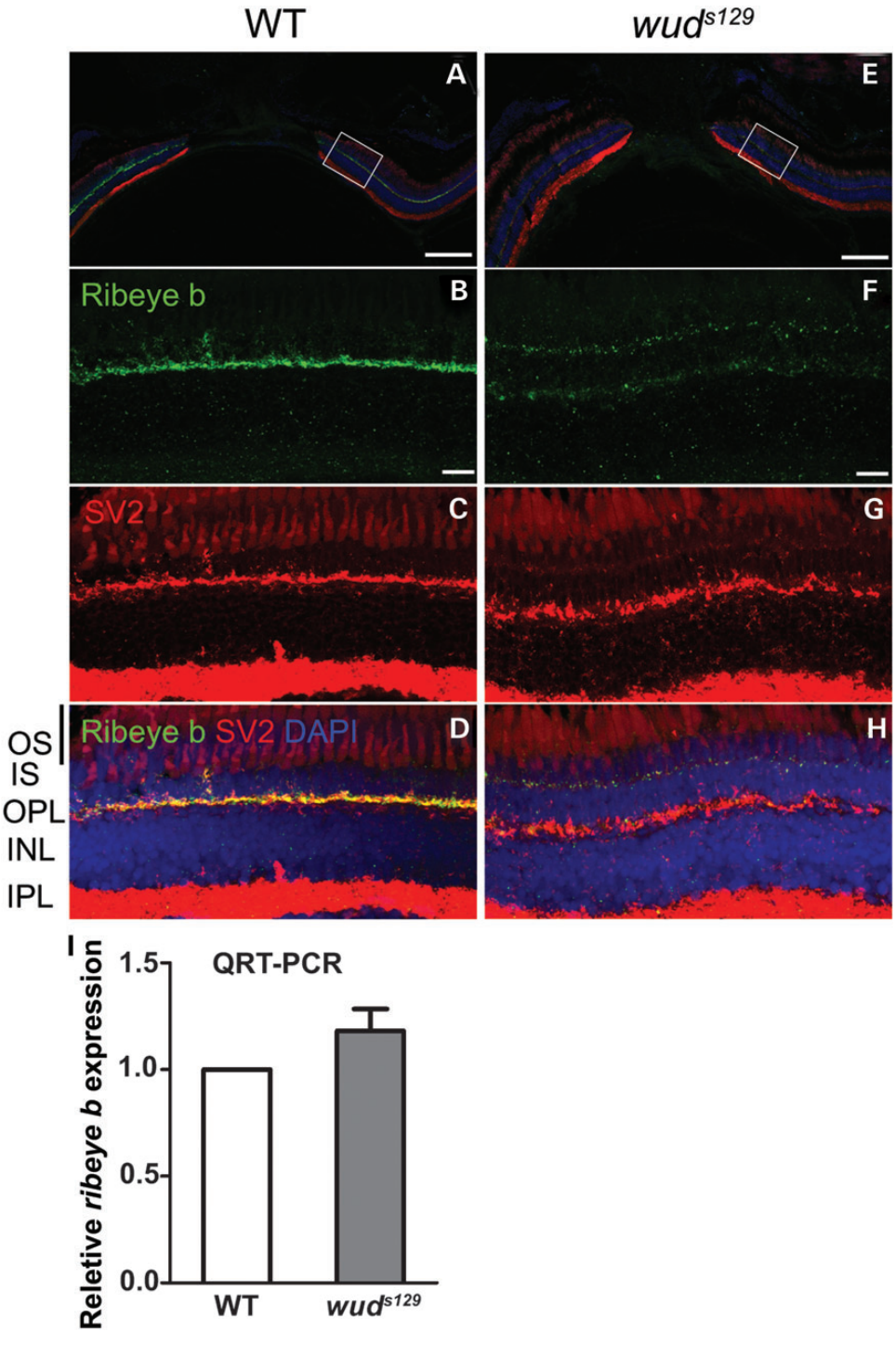

Figure 6. Ribeye b is reduced and mislocalized in *wud* mutants. (**A–H**) IHC was performed on 3-month-old wild-type and *wud* mutant retinas. Shown here is wild-type (A–D) and *wud* mutant (E–H) staining with Ribeye b (green), SV2 (red) and DAPI (blue). Close-ups are shown for the individual channels for Ribeye b (B, wild type; F, *wud*), SV2 (C, wild type; G, *wud*), and the overlay with DAPI (D, wild type; H, *wud*). (I) Quantitative RT-PCR indicated that the expression of ribeye b mRNA was normal in the wud retina relative to wild-type siblings. Error bars represent the standard error of the mean. Scale bar: (A) and (E), 100 μm; (B) and (F), 10 μm.

transmission in rods and cones are somewhat different as reflected in the variation in the number and size of synaptic ribbons. Thus, the cone-dominated retina along with the divergent expression pattern of *cacna1f* make the *wud* mutant a unique tool for studying the role of calcium channels in cone photoreceptor synapses.

Why is the ERG abnormal in *wud* mutants? Previous studies in mice have shown that mutations in photoreceptor calcium channels result in abnormal synaptic transmission in rod photoreceptors (20,27,40). While it would be predicted that mutations in zebrafish *cacna1fa* would result in defective synaptic transmission, we also uncovered a slow, positive-going component of

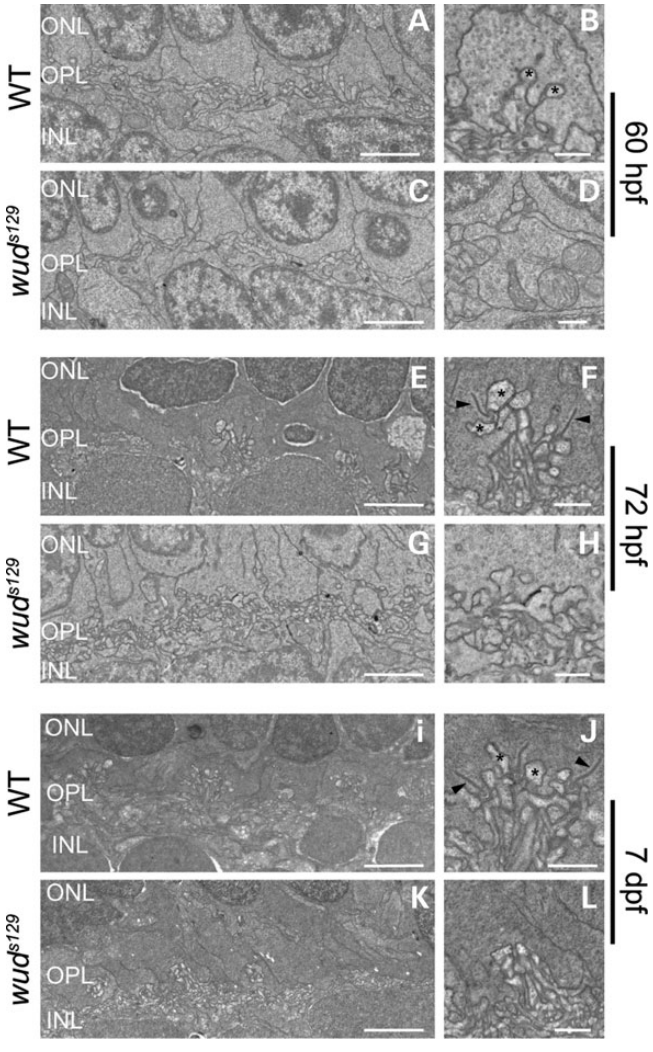

Figure 7. Cone synaptic ribbon formation is defective in *wud* mutants. Transmission electron microscopy of wild-type and *wud* mutant larvae during synaptic ribbon development. (**A**–**D**) At 60 hpf, no synaptic ribbons were observed in wild-type or *wud* mutants. Wild-type embryos showed the early stages of dendritic invagination into the cone pedicles (asterisks) (B), which was absent in the cone pedicles of *wud* mutants (D). At 72 hpf, wild-type embryos showed normal cone pedicles containing synaptic ribbons (**E** and **F**). *wud* mutants had abnormal cone pedicles and lacked synaptic ribbons (**G** and **H**), indicating a defect in the initial formation of synaptic ribbons. At 7 dpf, the results were similar to 72 hpf, where the wild-type larvae showed normal cone pedicles and synaptic ribbons (**I** and **J**) and *wud* mutants lacked synaptic ribbons (**K** and **L**). Arrowheads in (F) and (J) indicate synaptic ribbons. hpf, hours postfertilization; dpf, days postfertilization. Scale bar: (A), (C), (E), (G), (I) and (K), 2 μm; (B), (D), (F), (H), (J) and (L), 500 nm.

the ERG that resembled a c-wave. It is well documented that the c-wave originates in the retinal pigment epithelium (RPE) (41). Thus, it is possible that the retinal pigment is sensitized in *wud* mutants. Interestingly, no cone ERGs were elicited in mice with a loss-of-function mutation in Cacna1f (27). This is most likely due to cone photoreceptor degeneration in mouse mutants with a complete loss of Cacna1f (42). In contrast, human CSNB2 patients show variable cone ERGs (19), and no reports of cone degeneration have been reported in these patients. In fact, the cone ERGs from some of these individuals show a slow, positive-going component that somewhat resembles the *wud* mutant (19).

Alternatively, the abnormal ERG phenotype in *wud* could be explained by the genome duplication in zebrafish. Human and mouse contain a single *CACNA1F* gene that is expressed throughout many layers of the retina. In contrast, zebrafish have two *cacna1f* genes with *cacna1fa* (the *wud* gene) expressed in the photoreceptor layer and *cacna1fb* expressed in the inner retina. Perhaps the presence of *cacna1fb* in the inner retina elicits the slow, positive component of the *wud* ERG. While this remains a possibility, we did not see any change in the ERG phenotype when APB was applied (data not shown). This would indicate that the abnormal ERG arises upstream of the inner retina and supports the notion that this component is derived from cone photoreceptors or the RPE.

Here, we have reported the positional cloning of two blind zebrafish mutant lines with defective cone photoreceptor synaptic ribbons. *wud* mutants completely lack synaptic ribbons and *slak* mutants have floating synaptic ribbons. Both mutants provide a unique opportunity to dissect the formation of synaptic ribbons. In ribbon synapses, synaptic ribbons are attached at the arciform density via interactions with Bassoon (9). Synj1 also plays an important role in anchoring the ribbon to the plasma membrane, although the precise molecular mechanism remains unknown, as the components of the arciform density have not been identified. Perhaps Synj1 is a component of the arciform density, facilitating interactions with synaptic ribbon proteins such as Bassoon. This possibility could be interesting given that mouse *Bassoon* mutants also have floating ribbons (9).

In contrast to *slak* mutants, synaptic ribbons are completely missing in *wud* mutants (Fig. 5C and D). However, we did detect low levels of Ribeye b protein at the synaptic terminals and mislocalized Ribeye b in the inner segments (Fig. 6). Interestingly, we found no significant change in the mRNA level of *ribeye b*, indicating that the reduced expression is not transcriptionally regulated. While synaptic ribbons were absent in *wud* mutants, we did note the presence of putative srPB (Fig. 5C and D). This might suggest that some of the components necessary for synaptic ribbon formation are present, but that the assembly of ribbons is defective. Surprisingly, we found that Synj1 was absent in *wud* mutants, indicating that Cacna1fa and calcium influx may play a role in the regulation Synj1. Perhaps this form of regulation is important for other ribbon proteins, ultimately resulting in the loss of synaptic ribbons.

What role do L-VDCCs play in synaptic ribbon formation? One possibility is that L-VDCCs provide a structural scaffold for ribbon protein interactions. For example, structural defects at the photoreceptor synapse have previously been seen in mice with targeted disruption of synaptic ribbon-associated genes such as *Bassoon* (9) and *Pikachurin* (7). Recent studies have also shown that loss of either Bassoon or Ribeye affects the abundance or localization of L-type calcium channel ($Ca_v1.3$) in the hair cell ribbon synapse (31,43), indicating an intimate relationship between L-VDCCs and synaptic ribbon proteins. This has been further demonstrated in mouse double knockouts for P/Q- and N-type VDCCs where the expression of Bassoon and Piccolo was decreased at the presynaptic active zone of the neuromuscular junction (44). It has also been suggested that $Ca_v1.4$ may indirectly interact with synaptic ribbon proteins (45). For example, individual interactions between $Ca_v1.4$ and CaBP4 (46), CaBP4 and Munc119 (47) and Munc119 and Ribeye (48) could provide a mechanism for

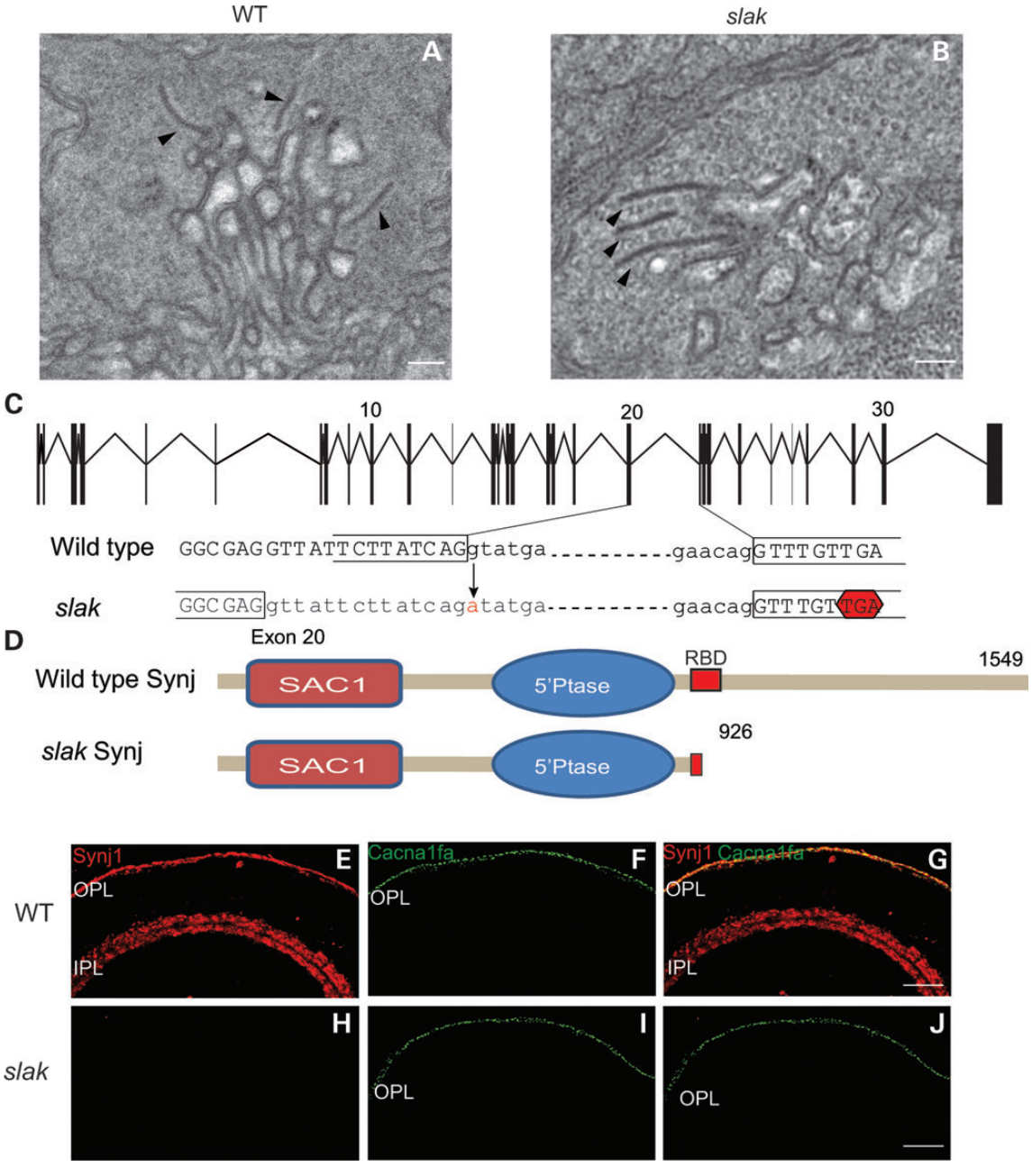

Figure 8. *slak*^{s564} encodes Synaptojanin 1 (Synj1). (**A** and **B**) Transmission electron microscopy showing normal ribbons in wild-type larvae (arrowheads in A) and floating ribbons in *slak* mutants at 7 dpf (arrowheads in B). (**C**) Schematic representation of the splice donor site mutation in *slak* that causes a frame shift in the coding sequence. The G to A mutation in *slak* results in a cryptic splice site 14 bp upstream of the original site and produces a premature stop codon. IHC of Synj1 and Cacna1f in *slak* mutants at 4 dpf. Synj1 is expressed in the OPL and IPL (**E** and **G**), whereas Cacna1fa is expressed only in the OPL (**F** and **G**) in wild type (WT). In *synj1* mutants, Synj1 is absent from both the OPL and IPL (**H** and **J**), whereas Cacna1fa is expressed in the OPL (**I** and **J**). Scale bar: (A) and (B), 500 nm; (G) and (J), 20 μm.

anchoring synaptic ribbon to calcium channels. However, if the only role for $Ca_v1.4$ was to provide a scaffold for synaptic ribbon anchoring, then we might have expected to see floating ribbons in the *wud* mutant, similar to what has previously been shown in the zebrafish *nrc* mutant (11) and our *slak* mutant.

Synaptic ribbon formation could also be regulated by L-VDCCs via calcium influx. Photoreceptor synaptic ribbons undergo activity-dependent changes due to the level of illumination (49), which has been shown to be dependent on the concentration of calcium and cGMP (50). For example, chelating intracellular calcium leads to disassembly of synaptic ribbons in photoreceptor cells (51). A recent study also suggested that the calcium sensor protein guanylyl cyclase-activating protein 2, GCAP2, is a prime candidate for mediating dynamic calcium-dependent changes in synaptic ribbons (52). While the direct relationship between calcium and synaptic ribbons remains unknown, it is well documented that calcium plays a vital role in neurotransmitter release, regulation of

calcium channel activity by calmodulin and CaBP4 (46,53), and calcium-dependent gene transcription (54). In addition, a recent study by Sheets *et al*. indicated that calcium influx through $Ca_v1.3$ channels regulate the assembly or accumulation of Ribeye protein in zebrafish sensory hair cells and pinealocytes (33). In this study, we demonstrated that Ribeye b is significantly downregulated and mislocalized in *wud* mutants and that the L-type calcium channel blocker isradipine disrupted the expression of the synaptic ribbon proteins Synj1 and Ribeye b. Taken together, it seems likely that calcium influx influences the structure and formation of synaptic ribbons and contributes to the loss of synaptic ribbons in the *wud* mutant.

Our cloning and characterization of the zebrafish *wud* mutant provides a valuable, non-mammalian model for dissecting the function of calcium channels in cone photoreceptors. The results from our phenotypic analysis in light of recent mouse studies lead us to propose that the absence of $Ca_v1.4$ in cones results in a complete loss of synaptic ribbons and indicates an essential role for calcium channels in the initial steps of synaptic ribbon development. Furthermore, our electrophysiological analysis demonstrated potentially additional functions of calcium channels in cone photoreceptors. Future studies with the *wud* mutant may further help to uncover the role that calcium channels play in regulating synaptic ribbon formation at the molecular level and ultimately may lead to insights into related human retinal diseases.

MATERIALS AND METHODS

Zebrafish strains and mutant identification

Zebrafish were raised and maintained under standard conditions. Larvae were kept in egg water (0.03% Instant Ocean reconstituted with reverse osmosis water) unless otherwise noted. Multiple alleles of the *wud* mutant and a single allele of *slacker*^{s564} (*slak*) were isolated from a large-scale mutagenesis screen for defects in visual behavior (22). For this study, we analyzed the *wud*^{s129}, *wud*^{s315} and *slak* alleles. For all experimental procedures, zebrafish were maintained in the TL strain. For genetic mapping experiments, heterozygous carriers of the *wud*^{s129} allele were crossed to the WIK strain. For complementation analysis, *slak* heterozygotes were bred to *no optokinetic response c* (*nrc*) heterozygotes (kindly provided by Dr. Susan Brockerhoff, University of Washington) (11). To identify wild-type and mutant larvae from an adult heterozygous cross, we measured the OKR as previously described (22,55). Larvae at 5–7 dpf were scored as wild type (OKR+) or mutant (OKR−) on the basis of their visual responses. For some IHC experiments, *wud*^{s129} larvae were obtained by *in vitro* fertilization using sperm and eggs collected from *wud* homozygous adults. Experiments on live animals were conducted in accordance with the guidelines of the St. Jude Children's Research Hospital Institutional Animal Care and Use Committee.

Histological analysis

Larvae were anesthetized in 0.02% tricaine, fixed in 4% paraformaldehyde in PBS at 4°C overnight or 30 min at room temperature, equilibrated in 30% sucrose in PBS, embedded into O.C.T. compound (Tissue-Tek) and sectioned at 15 μm on a cryostat (Leica). Sections were blocked in 5% normal goat serum, 0.3% Trixon X-100 in PBS and incubated with the following primary antibodies diluted in blocking buffer: anti-PKCβ1 (1 : 800 dilution; Santa Cruz Biotechnology), zpr-1 (1:200 dilution; Zebrafish International Resource Center), anti-SV2 (1:250 dilution, DSHB, University of Iowa) and anti-Ribeye b (1:250 dilution; kindly provided by Dr. Teresa Nicolson, Oregon Health & Science University), anti-Synj1 (undiluted; kindly provided by Dr. Susan Brockerhoff, University of Washington) and anti-Cacna1fa (1:6000 dilution). To produce the zebrafish Cacna1fa polyclonal antibody, we generated a GST-tagged, C-terminal fragment of Cacna1fa (amino acid 1581–1811) as an antigen, and Proteintech made the antibody in rabbit. Slides were washed in PBS three times for 10 min per wash and then incubated with Alexa488-, Alexa568- or Alexa 647-conjugated goat anti-mouse or anti-rabbit IgG (1:1000 dilution, Invitrogen) and counterstained with 4′,6-diamidino-2-phenylindole (DAPI; 1 μg/ml) for nuclear staining.

Semi-thin plastic sections

JB4 plastic sections were obtained as previously described (56). Wild-type and mutant larvae at 7 dpf were fixed in 4% paraformaldehyde at 4°C overnight. After being washed in PBS for several times, larvae were dehydrated in a stepwise series of ethanol in PBS (5, 25, 50, 75% ethanol in PBS) followed by a final dehydration in 100% ethanol. Ethanol was replaced with infiltration solution (JB-4 mini embedding kit, Polysciences Inc.), and exchanged with fresh infiltration solution when the larvae settled to the bottom of the tube. After overnight incubation, samples were embedded in JB-4 resin (JB-4 mini embedding kit, Polysciences Inc.). Sections (1 μm) were cut and stained with hematoxylin and eosin. Images were captured on a Nikon E800 microscope with Nikon DXM1200 camera and analyzed with NIS Elements AR3.0 software. Data were obtained from four wild type and four mutants. Two sections from each fish were measured at three regions close to the optical nerve for a total of 24 data points for each group. GraphPad Prism 5.0 (GraphPad Software) was used to perform unpaired *t*-test for statistical analyses.

Electroretinograms

Zebrafish larvae at 5–6 dpf were anesthetized by immersion in 0.02% tricaine in 0.09% Instant Ocean for 1 min before being gently placed on a moist sponge in an RC-10 recording chamber (Warner Instruments). The larvae were positioned so that one eye was facing the light stimulus. Glass recording electrodes were pulled on a P-97 micropipette puller (Sutter Instrument) and fire polished to a tip diameter of ∼20 μm using an MF-200 Micro-Forge (World Precision Instruments). The recording chamber and electrode were filled with 0.02% tricaine in 0.09% Instant Ocean. Before recording, the specimen was dark adapted for 10 min. The recording electrode was positioned directly on the cornea using a micromanipulator under infrared illumination. The reference electrode was placed in the adjacent ground reservoir. Light was generated from a 100-W QTH (quartz tungsten halogen) Oriel lamp housing and positioned 5 cm from the specimen using liquid light guides (Newport). The unattenuated light stimulus was set to 2 mW/cm^2.

A stimulus duration of 20 ms was controlled by a VCM-D1 Shutter Driver and VS25 Shutter (Uniblitz) using pCLAMP 10 software (Molecular Devices) and was attenuated using neutral density filters covering a range of 3 log units. The voltage signal was filtered by a Hum Bug 50/60 Hz noise eliminator (Quest Scientific), amplified with a DP-311 differential amplifier (settings: high pass of 0.1 Hz, low pass of 100 Hz and gain of 10^3; Warner Instruments), digitized with a Digidata 1440A (Molecular Devices) and acquired and analyzed with pCLAMP 10 software (Molecular Devices). Each trace is an average of six trials captured at 20 s intervals. All ERGs were performed at room temperature (22–24°C).

Genetic mapping and positional cloning

Genetic mapping was performed using microsatellite-based linkage mapping methods by bulked segregant analysis with 192 polymorphic primer pairs evenly distributed across the zebrafish genome. As previously described (22), *wud* was mapped to LG 8 and *slak* was mapped to LG 10. Fine mapping of *wud* defined a 4.7 Mb critical interval between markers z789 and z15786. Fine mapping of *slak* defined a 1.2 Mb critical interval between markers z7504 and z9574. To evaluate selected candidate genes, we sequenced cDNA from both mutants and their wild-type siblings. Total RNA was extracted from 20 wild-type (OKR+) and 20 mutant (OKR−) larvae using TRIzol (Invitrogen), cDNA was synthesized using the SuperScript III First Strand Synthesis Kit (Invitrogen), and PCR was performed in duplicate with overlapping DNA primer pairs specific to the open reading frame of the zebrafish gene being evaluated (primer sequences are available upon request). PCR products were run on a 1% agarose gel, extracted using a QIAquick Gel Extraction Kit (Qiagen), and sequenced.

Whole-mount *in situ* hybridization

WISH was performed as previously described (57). Briefly, larvae were fixed in 4% paraformaldehyde at 4°C overnight, dehydrated in 100% methanol and stored at −20°C. Larvae were rehydrated in PBS, permeabilized with proteinase K, prehybridized at 70°C for 2 h and hybridized with digoxignein (DIG)-labeled RNA probes at 70°C overnight. For probe synthesis, *cacna1fa* (nt 4642–6273) and *cacna1fb* (nt 5132–6622) were PCR amplified from wild-type zebrafish cDNA and cloned into the pCRII-TOPO Dual Promoter Vector (Invitrogen). Sense and antisense DIG-labeled RNA probes were synthesized with Sp6 and T7 RNA polymerase using a DIG RNA Labeling Kit (Roche). After washing and blocking, the larvae were incubated with anti-DIG-AP Fab fragment for 2 h and stained with BCIP/NBT substrate until the desired signal intensity appeared. Stained larvae were mounted in glycerol for imaging or embedded in O.C.T. compound, frozen on dry ice and sectioned at 10 μm using a Leica CM1950 cryostat.

Immunoblotting

Whole adult zebrafish eyes were homogenized in 100 μl homogenization buffer [cOmplete Proteinase Inhibitor Cocktail tablet (Roche) in 25 ml water] with a Pellet Pestle (Kontes). Laemmli sample buffer was added and the samples were boiled for 10 min. Proteins were separated on 4–12% Bio-Rad precast TGX gels and transferred to nitrocellulose membrane (Millipore). Membranes were blocked for 10 min in 10% non-fat dry milk (Sysco) in TBST, incubated with primary antibodies overnight at 4°C, followed by IRDye secondary antibodies diluted in Odyssey blocking buffer (LI-COR). Signals were detected with Odyssey Infrared Imaging System (LI-COR) at 680 and 800 nm. The primary antibodies used were mouse monoclonal against actin (1:6000, Proteintech) and rabbit polyclonal against Cacna1fa (1:500, Proteintech). The secondary antibodies used were anti-mouse IgG (IRDye 800) and anti-rabbit IgG (IRDye 680).

Transmission electron microscopy

Adult eyes or whole larvae (3–7 dpf) were fixed in 4% glutaraldehyde in 0.1 M sodium cacodylate buffer (pH 7.4) and post fixed in 2% osmium tetroxide in 0.1 M sodium cacodylate buffer with 0.3% potassium ferrocyanide for 2 h. The samples ($n = 4$ for adult eyes, $n = 3$ or 5 for whole larvae) were serially dehydrated in ethanol and then serially transferred to propylene oxide. Samples were infiltrated and embedded in epoxy resin and polymerized at 70°C overnight. Semi-thin sections (0.5 μm) were stained with toluidine blue for light microscope examination. Ultrathin sections (80 nm) were cut with a Leica EM UC6 Ultramicrotome and imaged using a JEOL 1200 electron microscope equipped with an AMT XR 111 camera.

Quantitative RT-PCR

Retinae were dissected from four individual adult zebrafish (4 months old). Both retinae from individual fish were pooled. Total RNA was prepared with TRIzol (Invitrogen) and was further purified with RNeasy columns (Qiagen) as described (58). cDNA was synthesized using QuantiTect Reverse Transcription Kit (Qiagen). Quantitative RT-PCR was performed using the SYBR Green PCR Master Mix (Applied Biosystems) in the Applied Biosystems 7900HT Fast Real-Time PCR System as described (59). Samples were analyzed in triplicate and normalized to β-actin. The following primers were used:

ribeye b forward: GCTTCAGCCACCGTAATGAT
ribeye b reserve: TTCCAGTAGATGCTGCGATG
β-*actin* forward: TGAATCCCAAAGCCAACAGAG
β-*actin* reverse: TCACACCATCACCAGAGTCC

Pharmacological blockade of calcium influx

Dark-adapted wild-type larvae at 7 dpf were exposed to light for 1 h (∼200 μW) in the presence of 0.1% DMSO/Embryo Medium (E3) (control) or 10 μM isradipine (Sigma I6658–5MG) in 0.1% DMSO/E3. Embryos were raised in darkness from 1 dpf until drug treatment. Following treatment, larvae were fixed in 4% paraformaldehyde, sectioned and examined by IHC.

SUPPLEMENTARY MATERIAL

Supplementary Material is available at *HMG* online.

ACKNOWLEDGEMENTS

We thank Dr Juan Korenbrot (UCSF) for help with electroretinograms, Sharon Frase and Yannan Ouyang of the Cell and Tissue Imaging Center at St. Jude Children's Research Hospital for their help with electron and confocal microscope, and members of the Taylor and Baier groups for help with mutagenesis screening and fish facility maintenance.

Conflict of Interest statement. None declared.

FUNDING

This work was supported by the Knights Templar Eye Foundation (S.J.), the National Institutes of Health (NIH) Grants EY12406 and EY13855 (H.B.) and the E. Matilda Ziegler Foundation for the Blind, St. Jude Children's Research Hospital and ALSAC (M.R.T.). Confocal microscopy and transmission electron microscopy were performed in the St. Jude Children's Research Hospital Cell & Tissue Imaging Center, which is supported by National Institutes of Health grant NCI P30 CA021765-34.

REFERENCES

1. Choi, S.Y., Borghuis, B.G., Rea, R., Levitan, E.S., Sterling, P. and Kramer, R.H. (2005) Encoding light intensity by the cone photoreceptor synapse. *Neuron*, **48**, 555–562.
2. Sterling, P. and Matthews, G. (2005) Structure and function of ribbon synapses. *Trends Neurosci.*, **28**, 20–29.
3. Schmitz, F. (2009) The making of synaptic ribbons: how they are built and what they do. *Neuroscientist*, **15**, 611–624.
4. tom Dieck, S. and Brandstatter, J.H. (2006) Ribbon synapses of the retina. *Cell Tissue Res.*, **326**, 339–346.
5. Zanazzi, G. and Matthews, G. (2009) The molecular architecture of ribbon presynaptic terminals. *Mol. Neurobiol.*, **39**, 130–148.
6. Jackman, S.L., Choi, S.Y., Thoreson, W.B., Rabl, K., Bartoletti, T.M. and Kramer, R.H. (2009) Role of the synaptic ribbon in transmitting the cone light response. *Nat. Neurosci.*, **12**, 303–310.
7. Sato, S., Omori, Y., Katoh, K., Kondo, M., Kanagawa, M., Miyata, K., Funabiki, K., Koyasu, T., Kajimura, N., Miyoshi, T. *et al.* (2008) Pikachurin, a dystroglycan ligand, is essential for photoreceptor ribbon synapse formation. *Nat. Neurosci.*, **11**, 923–931.
8. Stohr, H., Heisig, J.B., Benz, P.M., Schoberl, S., Milenkovic, V.M., Strauss, O., Aartsen, W.M., Wijnholds, J., Weber, B.H. and Schulz, H.L. (2009) TMEM16B, a novel protein with calcium-dependent chloride channel activity, associates with a presynaptic protein complex in photoreceptor terminals. *J. Neurosci.*, **29**, 6809–6818.
9. Dick, O., tom Dieck, S., Altrock, W.D., Ammermuller, J., Weiler, R., Garner, C.C., Gundelfinger, E.D. and Brandstatter, J.H. (2003) The presynaptic active zone protein bassoon is essential for photoreceptor ribbon synapse formation in the retina. *Neuron*, **37**, 775–786.
10. Allwardt, B.A., Lall, A.B., Brockerhoff, S.E. and Dowling, J.E. (2001) Synapse formation is arrested in retinal photoreceptors of the zebrafish nrc mutant. *J. Neurosci.*, **21**, 2330–2342.
11. Van Epps, H.A., Hayashi, M., Lucast, L., Stearns, G.W., Hurley, J.B., De Camilli, P. and Brockerhoff, S.E. (2004) The zebrafish nrc mutant reveals a role for the polyphosphoinositide phosphatase synaptojanin 1 in cone photoreceptor ribbon anchoring. *J. Neurosci.*, **24**, 8641–8650.
12. Trapani, J.G., Obholzer, N., Mo, W., Brockerhoff, S.E. and Nicolson, T. (2009) Synaptojanin1 is required for temporal fidelity of synaptic transmission in hair cells. *PLoS Genet.*, **5**, e1000480.
13. Holzhausen, L.C., Lewis, A.A., Cheong, K.K. and Brockerhoff, S.E. (2009) Differential role for synaptojanin 1 in rod and cone photoreceptors. *J. Comp. Neurol.*, **517**, 633–644.
14. Wan, L., Almers, W. and Chen, W. (2005) Two ribeye genes in teleosts: the role of Ribeye in ribbon formation and bipolar cell development. *J. Neurosci.*, **25**, 941–949.
15. Matthews, G. and Fuchs, P. (2010) The diverse roles of ribbon synapses in sensory neurotransmission. *Nat. Rev. Neurosci*, **11**, 812–822.
16. Bech-Hansen, N.T., Naylor, M.J., Maybaum, T.A., Pearce, W.G., Koop, B., Fishman, G.A., Mets, M., Musarella, M.A. and Boycott, K.M. (1998) Loss-of-function mutations in a calcium-channel alpha1-subunit gene in Xp11.23 cause incomplete X-linked congenital stationary night blindness. *Nat. Genet.*, **19**, 264–267.
17. Jalkanen, R., Mantyjarvi, M., Tobias, R., Isosomppi, J., Sankila, E.M., Alitalo, T. and Bech-Hansen, N.T. (2006) X linked cone-rod dystrophy, CORDX3, is caused by a mutation in the CACNA1F gene. *J. Med. Genet.*, **43**, 699–704.
18. Strom, T.M., Nyakatura, G., Apfelstedt-Sylla, E., Hellebrand, H., Lorenz, B., Weber, B.H., Wutz, K., Gutwillinger, N., Ruther, K., Drescher, B. *et al.* (1998) An L-type calcium-channel gene mutated in incomplete X-linked congenital stationary night blindness. *Nat. Genet.*, **19**, 260–263.
19. Miyake, Y., Yagasaki, K., Horiguchi, M., Kawase, Y. and Kanda, T. (1986) Congenital stationary night blindness with negative electroretinogram. A new classification. Arch. Ophthalmol., **104**, 1013–1020.
20. Chang, B., Heckenlively, J.R., Bayley, P.R., Brecha, N.C., Davisson, M.T., Hawes, N.L., Hirano, A.A., Hurd, R.E., Ikeda, A., Johnson, B.A. *et al.* (2006) The nob2 mouse, a null mutation in Cacna1f: anatomical and functional abnormalities in the outer retina and their consequences on ganglion cell visual responses. *Vis. Neurosci.*, **23**, 11–24.
21. Doering, C.J., Rehak, R., Bonfield, S., Peloquin, J.B., Stell, W.K., Mema, S.C., Sauve, Y. and McRory, J.E. (2008) Modified Ca(v)1.4 expression in the Cacna1f(nob2) mouse due to alternative splicing of an ETn inserted in exon 2. *PLoS ONE*, **3**, e2538.
22. Muto, A., Orger, M.B., Wehman, A.M., Smear, M.C., Kay, J.N., Page-McCaw, P.S., Gahtan, E., Xiao, T., Nevin, L.M., Gosse, N.J. *et al.* (2005) Forward genetic analysis of visual behavior in zebrafish. *PLoS Genet.*, **1**, e66.
23. Bilotta, J., Saszik, S. and Sutherland, S.E. (2001) Rod contributions to the electroretinogram of the dark-adapted developing zebrafish. *Dev. Dyn.*, **222**, 564–570.
24. Van Epps, H.A., Yim, C.M., Hurley, J.B. and Brockerhoff, S.E. (2001) Investigations of photoreceptor synaptic transmission and light adaptation in the zebrafish visual mutant nrc. *Invest. Ophthalmol. Vis. Sci.*, **42**, 868–874.
25. Stearns, G., Evangelista, M., Fadool, J.M. and Brockerhoff, S.E. (2007) A mutation in the cone-specific pde6 gene causes rapid cone photoreceptor degeneration in zebrafish. *J. Neurosci.*, **27**, 13866–13874.
26. Bayley, P.R. and Morgans, C.W. (2007) Rod bipolar cells and horizontal cells form displaced synaptic contacts with rods in the outer nuclear layer of the nob2 retina. *J. Comp. Neurol.*, **500**, 286–298.
27. Mansergh, F., Orton, N.C., Vessey, J.P., Lalonde, M.R., Stell, W.K., Tremblay, F., Barnes, S., Rancourt, D.E. and Bech-Hansen, N.T. (2005) Mutation of the calcium channel gene Cacna1f disrupts calcium signaling, synaptic transmission and cellular organization in mouse retina. *Hum. Mol. Genet.*, **14**, 3035–3046.
28. Schmitz, F., Konigstorfer, A. and Sudhof, T.C. (2000) RIBEYE, a component of synaptic ribbons: a protein's journey through evolution provides insight into synaptic ribbon function. *Neuron*, **28**, 857–872.
29. Regus-Leidig, H., Tom Dieck, S., Specht, D., Meyer, L. and Brandstatter, J.H. (2009) Early steps in the assembly of photoreceptor ribbon synapses in the mouse retina: the involvement of precursor spheres. *J. Comp. Neurol.*, **512**, 814–824.
30. Magupalli, V.G., Schwarz, K., Alpadi, K., Natarajan, S., Seigel, G.M. and Schmitz, F. (2008) Multiple RIBEYE-RIBEYE interactions create a dynamic scaffold for the formation of synaptic ribbons. *J. Neurosci.*, **28**, 7954–7967.
31. Sheets, L., Trapani, J.G., Mo, W., Obholzer, N. and Nicolson, T. (2011) Ribeye is required for presynaptic CaV1.3a channel localization and afferent innervation of sensory hair cells. *Development*, **138**, 1309–1319.
32. Catterall, W.A. (2011) Voltage-gated calcium channels. *Cold Spring Harb. Perspect. Biol.*, **3**, a003947.
33. Sheets, L., Kindt, K.S. and Nicolson, T. (2012) Presynaptic CaV1.3 channels regulate synaptic ribbon size and are required for synaptic maintenance in sensory hair cells. *J. Neurosci.*, **32**, 17273–17286.
34. Wagner, H.J. (1973) Darkness-induced reduction of the number of synaptic ribbons in fish retina. Nature, **246**, 53–55.

35. Nicolson, T., Rusch, A., Friedrich, R.W., Granato, M., Ruppersberg, J.P. and Nusslein-Volhard, C. (1998) Genetic analysis of vertebrate sensory hair cell mechanosensation: the zebrafish circler mutants. *Neuron*, **20**, 271–283.
36. Boycott, K.M., Maybaum, T.A., Naylor, M.J., Weleber, R.G., Robitaille, J., Miyake, Y., Bergen, A.A., Pierpont, M.E., Pearce, W.G. and Bech-Hansen, N.T. (2001) A summary of 20 CACNA1F mutations identified in 36 families with incomplete X-linked congenital stationary night blindness, and characterization of splice variants. *Hum. Genet.*, **108**, 91–97.
37. Boycott, K.M., Pearce, W.G. and Bech-Hansen, N.T. (2000) Clinical variability among patients with incomplete X-linked congenital stationary night blindness and a founder mutation in CACNA1F. *Can. J. Ophthalmol.*, **35**, 204–213.
38. Jacobi, F.K., Andreasson, S., Langrova, H., Meindl, A., Zrenner, E., Apfelstedt-Sylla, E. and Pusch, C.M. (2002) Phenotypic expression of the complete type of X-linked congenital stationary night blindness in patients with different mutations in the NYX gene. *Graefes Arch. Clin. Exp. Ophthalmol.*, **240**, 822–828.
39. Lodha, N., Bonfield, S., Orton, N.C., Doering, C.J., McRory, J.E., Mema, S.C., Rehak, R., Sauve, Y., Tobias, R., Stell, W.K. *et al.* (2010) Congenital stationary night blindness in mice – a tale of two Cacna1f mutants. *Adv. Exp. Med. Biol.*, **664**, 549–558.
40. Ball, S.L., Powers, P.A., Shin, H.S., Morgans, C.W., Peachey, N.S. and Gregg, R.G. (2002) Role of the beta(2) subunit of voltage-dependent calcium channels in the retinal outer plexiform layer. *Invest. Ophthalmol. Vis. Sci.*, **43**, 1595–1603.
41. Perlman, I. (1995) The Electroretinogram: ERG. Kolb, H., Fernandez, E. and Nelson, R. (eds.), In *Webvision: The Organization of the Retina and Visual System*. WordPress, Salt Lake City, UT.
42. Michalakis, S., Shaltiel, L., Sothilingam, V., Koch, S., Schludi, V., Krause, S., Zeitz, C., Audo, I., Lancelot, M.E., Hamel, C. *et al.* (2014) Mosaic synaptopathy and functional defects in Cav1.4 heterozygous mice and human carriers of CSNB2. *Hum. Mol. Genet.*, **23**, 1538–1550.
43. Frank, T., Rutherford, M.A., Strenzke, N., Neef, A., Pangrsic, T., Khimich, D., Fetjova, A., Gundelfinger, E.D., Liberman, M.C., Harke, B. *et al.* (2010) Bassoon and the synaptic ribbon organize Ca(2+) channels and vesicles to add release sites and promote refilling. *Neuron*, **68**, 724–738.
44. Chen, J., Billings, S.E. and Nishimune, H. (2011) Calcium channels link the muscle-derived synapse organizer laminin beta2 to Bassoon and CAST/Erc2 to organize presynaptic active zones. *J. Neurosci.*, **31**, 512–525.
45. Schmitz, F., Natarajan, S., Venkatesan, J.K., Wahl, S., Schwarz, K. and Grabner, C.P. (2012) EF hand-mediated Ca- and cGMP-signaling in photoreceptor synaptic terminals. *Front. Mol. Neurosci.*, **5**, 26.
46. Haeseleer, F., Imanishi, Y., Maeda, T., Possin, D.E., Maeda, A., Lee, A., Rieke, F. and Palczewski, K. (2004) Essential role of Ca2+-binding protein 4, a Cav1.4 channel regulator, in photoreceptor synaptic function. *Nat. Neurosci.*, **7**, 1079–1087.
47. Haeseleer, F. (2008) Interaction and colocalization of CaBP4 and Unc119 (MRG4) in photoreceptors. *Invest. Ophthalmol. Vis. Sci.*, **49**, 2366–2375.
48. Alpadi, K., Magupalli, V.G., Kappel, S., Koblitz, L., Schwarz, K., Seigel, G.M., Sung, C.H. and Schmitz, F. (2008) RIBEYE recruits Munc119, a mammalian ortholog of the Caenorhabditis elegans protein unc119, to synaptic ribbons of photoreceptor synapses. *J. Biol. Chem.*, **283**, 26461–26467.
49. Spiwoks-Becker, I., Glas, M., Lasarzik, I. and Vollrath, L. (2004) Mouse photoreceptor synaptic ribbons lose and regain material in response to illumination changes. *Eur. J. Neurosci.*, **19**, 1559–1571.
50. Vollrath, L. and Spiwoks-Becker, I. (1996) Plasticity of retinal ribbon synapses. *Microsc. Res. Tech.*, **35**, 472–487.
51. Regus-Leidig, H., Specht, D., Tom Dieck, S. and Brandstatter, J.H. (2010) Stability of active zone components at the photoreceptor ribbon complex. *Mol. Vis.*, **16**, 2690–2700.
52. Venkatesan, J.K., Natarajan, S., Schwarz, K., Mayer, S.I., Alpadi, K., Magupalli, V.G., Sung, C.H. and Schmitz, F. (2010) Nicotinamide adenine dinucleotide-dependent binding of the neuronal Ca2+ sensor protein GCAP2 to photoreceptor synaptic ribbons. *J. Neurosci.*, **30**, 6559–6576.
53. Dolmetsch, R.E., Pajvani, U., Fife, K., Spotts, J.M. and Greenberg, M.E. (2001) Signaling to the nucleus by an L-type calcium channel-calmodulin complex through the MAP kinase pathway. *Science*, **294**, 333–339.
54. Wheeler, D.G., Groth, R.D., Ma, H., Barrett, C.F., Owen, S.F., Safa, P. and Tsien, R.W. (2012) Ca(V)1 and Ca(V)2 channels engage distinct modes of Ca(2+) signaling to control CREB-dependent gene expression. *Cell*, **149**, 1112–1124.
55. Brockerhoff, S.E., Hurley, J.B., Janssen-Bienhold, U., Neuhauss, S.C., Driever, W. and Dowling, J.E. (1995) A behavioral screen for isolating zebrafish mutants with visual system defects. *Proc. Natl. Acad. Sci. USA*, **92**, 10545–10549.
56. Sullivan-Brown, J., Bisher, M.E. and Burdine, R.D. (2011) Embedding, serial sectioning and staining of zebrafish embryos using JB-4 resin. *Nat. Protoc.*, **6**, 46–55.
57. Thisse, C. and Thisse, B. (2008) High-resolution in situ hybridization to whole-mount zebrafish embryos. *Nat. Protoc.*, **3**, 59–69.
58. Leung, Y.F. and Dowling, J.E. (2005) Gene expression profiling of zebrafish embryonic retina. *Zebrafish*, **2**, 269–283.
59. Jia, S., Omelchenko, M., Garland, D., Vasiliou, V., Kanungo, J., Spencer, M., Wolf, Y., Koonin, E. and Piatigorsky, J. (2007) Duplicated gelsolin family genes in zebrafish: a novel scinderin-like gene (scinla) encodes the major corneal crystallin. *FASEB J.*, **21**, 3318–3328.